

Real-time Model Predictive Control and System Identification Using Differentiable Physics Simulation

Sirui Chen[†], Keenon Werling^{*}, C. Karen Liu^{*}

^{*} Stanford University: {keenon, karenliu}@stanford.edu

[†] The University Of Hong Kong: {ericcsr}@connect.hku.hk

Abstract—Developing robot controllers in a simulated environment is advantageous but transferring the controllers to the target environment presents challenges, often referred to as the “sim-to-real gap”. We present a method for continuous improvement of modeling and control *after* deploying the robot to a dynamically-changing target environment. We develop a differentiable physics simulation framework that performs on-line system identification and optimal control simultaneously, using the incoming observations from the target environment in real time. To ensure robust system identification against noisy observations, we devise an algorithm to assess the confidence of our estimated parameters, using numerical analysis of the dynamic equations. To ensure real-time optimal control, we adaptively schedule the optimization window in the future so that the optimized actions can be replenished faster than they are consumed, while staying as up-to-date with new sensor information as possible. The constant re-planning based on a constantly improved model allows the robot to swiftly adapt to the changing environment and utilize real-world data in the most sample-efficient way. Thanks to a fast differentiable physics simulator, the optimization for both system identification and control can be solved efficiently for robots operating in real time. We demonstrate our method on a set of examples in simulation and show that our results are favorable compared to baseline methods.

I. Introduction

Simulation provides a valuable virtual testbed that allows the design and control stacks of the robot to be developed and evaluated in a risk-free manner. The major caveat, however, is that using simulation in robotics often leads to control policies or mechanical designs that fail when deployed in the real world, the *sim-to-real gap*. Much existing work has focused on training more robust and adaptive control policies in simulation, *prior to* crossing the sim-to-real gap [2]. In contrast, our work focuses on continuous improvement of modeling and control in the real world, *after* deploying the robot to the dynamically-changing target environment.

In this work, we address the problem of post-deployment fine-tuning from both modeling and control perspectives. We develop a differentiable physics simulation framework that performs online motion planning and system identification simultaneously as shown in 1, using the incoming observations in real time. Our system runs two parallel computation threads: a planning thread that solves for a sequence of actions over a finite horizon of time into the *future*, and concurrently, the modeling thread that optimizes the system parameters based

on the most recent *history* of observations. The constant re-planning based on a constantly improved model allows the robot to swiftly adapt to the changing environment and utilize the real-world data in the most sample-efficient way.

The main technical challenge in online system identification of a dynamically changing environment is that the observations might be outdated (when the environment actually changed) or uninformative (the observations were not “parametrically exciting”). These two scenarios lead to a very similar consequence—unstable and erroneous estimation of the system parameters—but call for very different solutions. We develop an adaptive online system identification method that monitors the changes in the environment and assesses the confidence of our estimated parameters, using numerical analysis of the dynamic equations. In addition, when the model is inaccurate, our dual-threaded framework provides a unique opportunity to actively control a trajectory for the purpose of system identification. That is, we can exploit the parallel planning thread to assist the system identification by producing parametrically exciting observations.

On the other hand, the main technical challenge for the planning thread is to replenish the planned action buffer faster than realtime while keeping the plan as fresh as possible. This is an interesting scheduling problem that can be solved by careful considerations of planning algorithms and problem formulation. We devise a procedure to solve the scheduling problem that balances the accuracy of the model and the computation complexity of the plan. In addition, we leverage the incremental replanning nature of model-predictive-control to improve the computational performance of the optimal control algorithm.

We evaluate our method on a number of simulated examples to demonstrate the effectiveness of our dual-threaded framework for planning and modeling. We compare our method with four baseline methods and evaluate them by the accuracy of system identification and effectiveness of control. Our results are favorable compared to all baselines.

II. Related Work

Deep reinforcement learning and model-based methods for robot control have both demonstrated impressive results in simulated environments. However, transferring controllers from simulated environment to real robot systems often fail due to

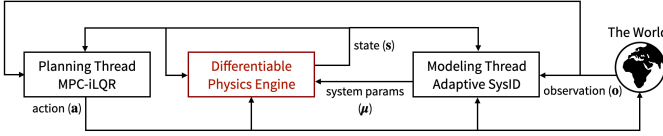


Fig. 1: A differentiable physics simulation framework that performs online motion planning and system identification simultaneously.

the sim-to-real gap [27], which has been an active research problem in recent years. Prior work has explored two different approaches to mitigate the sim-to-real gap: 1) Improving the accuracy and fidelity of robot models and simulators 2) Making the control policy more robust and adaptive to uncertainty or changes in system parameters.

A. Improve modeling accuracy

System identification (SysID) for robotic systems has been an important research area in robotics for decades. Classical methods for system identification, including the frequency response method and the impulse response method [1], probe the system parameter offline using characteristic input signals. System parameters can also be identified by solving a regression problem for both linear systems [18] and nonlinear ones [5]. Offline SysID has been applied in identifying bending and stretching stiffness of cloth [24] and masses of articulated 2D multi-body systems [3]. However, these methods are designed for identifying constant system parameters prior to deployment. For online SysID using incoming observations, recursive least square methods have been used for identifying linear systems [18]. Recent development of learning-based approaches have attempted different directions in improving modeling accuracy and may allow us to model unknown time-varying components. For example, Yu et al. [44] learned a neural network to infer system parameters using recent sensor observations, which can model time varying parameters. Jiang et al. [17] formulated system parameters as functions of state and action which can be learned from the real-world trajectories. Our adaptive system identification method is designed to run online and handle noisy state and action trajectories. Unlike learning-based methods, our online SysID does not require offline training using a large amount of data.

B. Adaptive control

Designing more adaptive and robust controllers is an effective way to tackle sim-to-real problems. For linear systems, model reference adaptive control (MRAC) [20] aims to minimize model matching error by optimizing controller gains, or using a Lyapunov function to verify stability [29]. In the robust control domain, Lyapunov functions [38] can be used to analyze a robust control policy, but Lyapunov function design for complex non-linear systems remains a challenging problem. Recently, researchers have demonstrated that reinforcement learning can be an effective tool to learn robust or adaptive control policies. Domain randomization of simulation parameters has been used to transfer policies trained in simulation to different target

environments [30, 37, 16, 6, 28]. However, policies trained with domain randomization tend to trade off task performance for robustness, resulting in over-conservative behaviors [37]. Learning adaptive control policies that can adjust behaviors for different environments using an estimation of the environment parameters is also a promising direction for sim-to-real transfer [36, 9, 43, 44, 31]. Our method is mostly related to Yu et al. [44] who proposed a method that trains a universal policy conditioned on the model parameters, which are identified by another learned system identification function. Our evaluation shows that our method achieves better task performance and system identification accuracy compared to the prior work.

C. Differentiable physics

In the last few years, various differentiable physics simulators have been proposed by researchers aiming to build better simulation tools for robotic tasks such as control, design and parameter identification. A significant amount of work focused on rigid body simulation [19, 4, 14, 11, 3, 33] with efficient formulations for contact [7, 41, 46, 34, 42, 21] and constraints [25]. Soft body simulation has also been made differentiable [35, 24, 8, 13, 33, 12, 7, 10] and tested on different robotic tasks [15] and hardware [40]. Roboticians have demonstrated that differentiable physics simulation can effectively identify simulation parameters [4, 14, 46, 10, 40, 21], optimize design parameters [7, 42, 25], or learn a hybrid simulator which combine learnable neural networks with differential equations [11, 32]. The gradient information can also be exploited in motion optimization [41, 10] and policy learning [34, 45]. The unique aspect of our method is that we utilize the gradients provided by a differentiable physics simulator simultaneously for control and system identification in an online fashion. This dual-purpose framework allows a robot to continue to adapt to an ever-changing environment in a sample efficient manner.

III. Method

We propose a new method that utilizes differentiable physics simulation for online system identification and optimal control of robots using streaming observations from the target environment. Our framework runs two parallel computation threads in real-time, a *planning thread* for optimal control and a *modeling thread* for system identification. The planning thread solves for a sequence of actions over a finite horizon of time into the *future*. Concurrently, the modeling thread optimizes the system parameters, μ , based on the most recent *history* of observations.

Figure 2 illustrates the communication and scheduling between the two threads. The modeling thread takes the state sequence in the history buffer \mathcal{H} that stores the most recent observed states from the target environment, optimizes μ to match \mathcal{H} via the gradients provided by the differentiable physics engine, and finally updates the engine itself with the optimal μ . As soon as it completes the optimization, it fetches the next batch of states from \mathcal{H} and repeats the optimization of μ . Asynchronously, the planning thread solves a future action sequence using the differentiable physics engine with the most recently updated μ . The planning thread formulates an optimal

control problem as an iterative linear quadratic regulator (iLQR) and solves it in a model-predictive-control (MPC) fashion. The solved action trajectory is placed in the plan buffer \mathcal{P} for the robot to consume in real-time. The next optimal control problem starts immediately after the current one is done with an optimization horizon that begins from some future state.

A. Real-time optimal control

Real-time optimal control problem could be formulated as a non-linear program and solved by a general optimization packages (e.g. IPOPT [39]). While the solutions could be reasonable, the computation time of each solution can vary wildly, which is not ideal for real-time applications. Alternatively, one could formulate the optimization as iLQR [23] or DDP [26] to solve for a fixed-horizon trajectory with more predictable computation time. With an efficient differentiable physics engine, our method is applicable to both optimal control approaches, but we prefer iLQR because the computation performance is more predictable for our control tasks. To achieve real-time optimal control, the computation speed of MPC-iLQR can be significantly improved by warm-starting the overlapping time window using the previous plan. Specifically, we initialize the linear control laws, the state trajectory, and

the action trajectory using the previous solution. The details of our MPC-iLQR formulation can be found in the Appendix VI-A.

The main technical challenge for the planning thread is to replenish the plan buffer \mathcal{P} faster than real-time while keeping the plan as fresh as possible. We propose to adaptively select the starting time \hat{t} of the horizon H of the trajectories being optimized: $\mathbf{x}_{\hat{t}:\hat{t}+H}, \mathbf{u}_{\hat{t}:\hat{t}+H-1}$. Ideally we would like \hat{t} to be as close as possible to the time index when the trajectory optimization is finished, so the new plan $\mathbf{u}_{\hat{t}:\hat{t}+H-1}$ will be fresh and just-in-time. If \hat{t} is too early, some of the new plan will be stale already by the time the planning is done. If \hat{t} is too late, the robot cannot switch to the new plan when the old one is depleted, leading to potentially sub-optimal behaviors.

We profile the computational time of the planning algorithm running on the target hardware to obtain the elapsed time t_e for each iLQR iteration. During runtime, we determine \hat{t} by multiplying the number of iterations, N_{iter} , the previous iLQR took with t_e : $\hat{t} = t + t_e \cdot N_{iter}$, where t is the current time index (Algorithm 1).

B. Real-time system identification

Given a sequence of recently observed states, $\mathbf{x} = [\mathbf{q}_{0:T}, \dot{\mathbf{q}}_{0:T}]$, in the history buffer \mathcal{H} , a standard system identification routine finds the optimal system parameters that best fit the observations: $\boldsymbol{\mu}^* = \arg \min_{\boldsymbol{\mu}} \|\text{sim}(\mathbf{q}_0, \dot{\mathbf{q}}_0; \boldsymbol{\mu}, T) - \mathbf{q}_{0:T}\|$, where $\text{sim}(\mathbf{q}_0, \dot{\mathbf{q}}_0; \boldsymbol{\mu}, T)$ is the forward simulation starting from state $(\mathbf{q}_0, \dot{\mathbf{q}}_0)$ for T time steps under the differential equations parameterized by $\boldsymbol{\mu}$. Utilizing a differential physics simulator (e.g. NimblePhysics [41]), we can compute the gradients of the objective function efficiently to optimize $\boldsymbol{\mu}$ in real time.

However, unlike a one-time offline SysID routine, repeatedly applying online SysID using incoming noisy observations in a dynamically changing environment often leads to erroneous and unstable estimation of system parameters. The main challenge of online SysID is that the observations might be outdated (when the environment actually changed) or uninformative (the observations were not “parametrically exciting”). The former requires the system to flush old observations in the buffer and only use the recent observations, while the latter can be mitigated by weighing the old observations more highly than the recent ones. Knowing which failure mode we are currently in is critical for the system to respond correctly.

We develop an adaptive online SysID method, inspired by the idea of persistent excitation analysis, to assess how a state trajectory spans the range of system behaviors. For each SysID optimization problem, we compute a confidence score, w and weight the solution by the confidence score. The currently estimated system parameter is defined as the weighted sum of solutions found in the past:

$$\bar{\boldsymbol{\mu}} = \frac{\sum_{i=1} w_i \boldsymbol{\mu}_i}{\sum_{i=1} w_i}. \quad (1)$$

At the end of each SysID optimization, we analyze the solution $\boldsymbol{\mu}^*$ and the confidence score w^* to determine the appropriate action. If w^* is high and $\|\boldsymbol{\mu}^* - \bar{\boldsymbol{\mu}}\|$ is low (i.e. the new solution is similar to the current one), we happily

Algorithm 1: Online SysID and Control

```

Input:  $\mathcal{H}, \mathcal{P}$ 
 $f \leftarrow f_{task}$ 
 $\bar{\boldsymbol{\mu}} \leftarrow \text{default\_value}()$ 
 $\bar{w} = 0; n = 0$ 
▷ Planning Thread:

while true do
   $t \leftarrow \text{current\_time}()$ 
   $\hat{t} = t + t_e \cdot N_{iter}$ 
   $\mathbf{x}_{\hat{t}:\hat{t}} \leftarrow \text{sim}(\mathbf{x}_t; \bar{\boldsymbol{\mu}}, \hat{t} - t)$ 
   $\mathbf{u}_{\hat{t}:\hat{t}+H-1} \leftarrow \text{iLQR}(\mathbf{x}_{\hat{t}}; \bar{\boldsymbol{\mu}}, H, f)$ 
   $\mathcal{P} \leftarrow \text{update}(\mathcal{P}, \mathbf{u}_{\hat{t}:\hat{t}+H-1})$ 
▷ Modeling Thread:

while true do
   $\mathbf{x}_{0:T} \leftarrow \text{recent\_batch}(\mathcal{H})$ 
   $\boldsymbol{\mu}^* = \arg \min_{\boldsymbol{\mu}} \|\text{sim}(\mathbf{x}_0; \boldsymbol{\mu}, T) - \mathbf{x}_{0:T}\|$ 
   $w^* \leftarrow \text{confidence\_score}(\mathbf{x}_{0:T})$ 
  if  $|w^*| > \epsilon_1$  then
     $f \leftarrow t_{task}$ 
    if  $\|\boldsymbol{\mu}^* - \bar{\boldsymbol{\mu}}\| < \epsilon_2$  then
       $\bar{\boldsymbol{\mu}} = \bar{\boldsymbol{\mu}} \frac{\bar{w}}{\bar{w} + w^*} + \boldsymbol{\mu}^* \frac{w^*}{\bar{w} + w^*}$ 
       $\bar{w} = \bar{w} + w^*$ 
    else
       $\bar{\boldsymbol{\mu}} = \boldsymbol{\mu}^*$ 
       $\bar{w} = w^*$ 
  else
     $n \leftarrow n + 1$ 
    if  $n > N_{his}$  then
       $f \leftarrow f_{exp}$ 
       $n = 0$ 

```

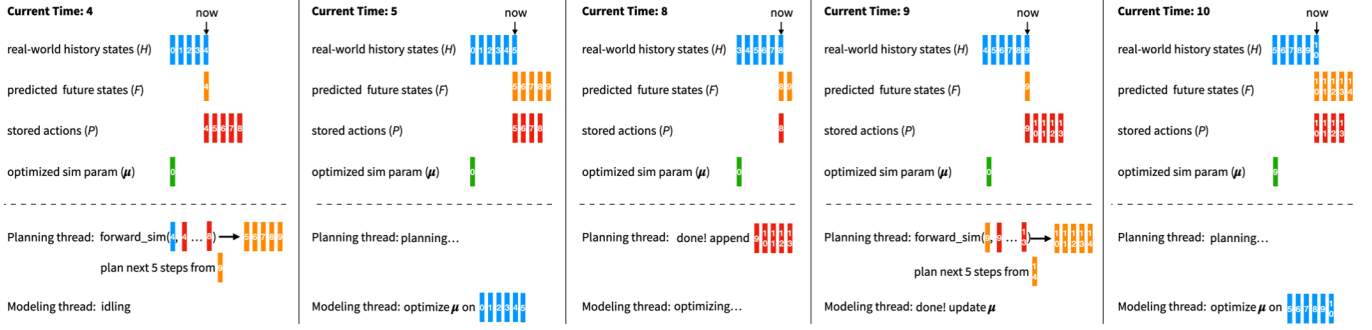


Fig. 2: Illustration of our dual-threaded real-time system. At the beginning of time step 4, the history buffer has accumulated five past state, $x_{0:4}$ (blue vectors) and the stored plan buffer has 5 actions $u_{4:8}$ (red vectors). The system parameters μ were last updated at time step 0 (green vector). Assuming the starting time step and the length of planning horizon is $\hat{t} = 5$ and $H = 5$ respectively. The planning thread first simulates 5 time steps forward and starts a trajectory optimization from x_9 . The modeling thread is waiting for the history buffer to fill up. At the beginning of time step 5, the history buffer is full so the modeling thread starts optimizing μ . The planning thread continues to solve the trajectory optimization. At time step 8, the planning thread is done with the new actions $u_{9:13}$ while the modeling thread continues to optimize μ . At time step 9, the robot starts to consume the new plan while a new trajectory optimization is spawned by the planning thread. The modeling thread finishes optimizing μ and updates the simulator at time step 10.

accept the new solution μ^* and update $\bar{\mu}$ using Equation 1. If w^* is high and $\|\mu^* - \bar{\mu}\|$ is also high, it is likely that the environment has changed and we need to re-estimate μ from scratch. In that case, we replace $\bar{\mu}$ with μ^* . If w^* is low, we discard μ^* and do not update $\bar{\mu}$. If low w^* persists for a N_{his} SysID optimizations, we switch to active SysID mode and change the objective function in the planning thread (details in Section III-C). Algorithm 1 summarizes both the adaptive online SysID and optimal control.

To compute the confidence score w , we leverage the Lagrange's equations of motion for articulated rigid body systems to estimate the parametric excitation for each system parameter:

$$M(q; \mu)\ddot{q} + c(q, \dot{q}; \mu) + g(q; \mu) = f(q, \dot{q}; \mu), \quad (2)$$

where M is the mass matrix in generalized coordinates $q \in \mathbb{R}^N$, c is the Coriolis and centrifugal force, g is the gravitational force, and f is the sum of other generalized forces applied on the system. While the actual formula to compute w for each system parameter is different, the underlying principle is the same. We will introduce the formulations for a few common parameters below.

a) Confidence score for estimating masses

To factor out the mass of each link, m_k , we rewrite Equation 2 as a linear function of $m = [m_1, \dots, m_M]$, where M is the number of rigid links in the system. For clarity of exposition, we omit the Coriolis and centrifugal force but provide detailed derivation in the Appendix VI-B.

$$(A(q, \ddot{q}) + B(q))m = f, \quad (3)$$

where the column k in $A \in \mathbb{R}^{N \times N}$ represents the acceleration of the rigid link k due to the inertial force in the generalized

coordinates: $A(:, k) = (J_k^T J_k + J_{\omega k}^T \tilde{I}_k J_{\omega k})\ddot{q} \in \mathbb{R}^{N \times 1}$. $\tilde{I}_k \in \mathbb{R}^{3 \times 3}$ is the inertia matrix in the coordinate frame of link k with the mass m_k factored out. The Jacobian matrix for the rigid link k contains two parts: the linear Jacobian $J_k \in \mathbb{R}^{3 \times N}$ and the angular Jacobian $J_{\omega k} \in \mathbb{R}^{3 \times N}$ which together map \dot{q} to the linear velocity and the angular velocity of link k in the Cartesian space. Similarly, the column k in B represents the acceleration of the rigid link k due to the gravitational force in the generalized coordinates: $B(:, k) = J_k^T g_e \in \mathbb{R}^N$, where $g_e = (0, 0, -9.8)^T$.

If the observations happen to make the rank of $A + B$ less than M , we cannot uniquely identify the mass for all M links. However, solving the rank for each time step and for each rigid link can be time consuming. We opt to use a heuristic that measures the magnitude of each column in $A + B$. When $\|A(:, k) + B(:, k)\|$ is small, the estimate of m_k is more sensitive to the sensing noise. If $\|A(:, k) + B(:, k)\|$ is zero, we lose the rank to identify m_k altogether. As such, the confidence score for estimating mass is defined as:

$$w = \sum_{t=0}^{T-1} \sum_{k=0}^{M-1} \left\| \frac{1}{\Delta t} (J_k^T J_k + J_{\omega k}^T \tilde{I}_k J_{\omega k}) (\dot{q}_{t+1} - \dot{q}_t) + J_k^T g_e \right\|,$$

where Δt is the simulation time step. All the Jacobian matrices are readily available from our differentiable physics engine [41].

b) Confidence score for estimating moment of inertia

Estimating the moment of inertia of each rigid link is also common for system identification. In our confidence score computation, we do not consider the off-diagonal elements in the local inertia matrix I_k , as they are typically dominated

¹We loosely use the matrix indexing notation $(:, k)$ to indicate the column k of the matrix.

by the diagonal elements (the principle inertia). Rearranging Equation 2 to factor out the principle inertia terms, $\mathbf{d}_k = (I_k^{xx}, I_k^{yy}, I_k^{zz})$, for each link k , we arrive at:

$$\begin{bmatrix} \mathbf{C}_1(\mathbf{q}, \ddot{\mathbf{q}}) & \cdots & \mathbf{C}_M(\mathbf{q}, \ddot{\mathbf{q}}) \end{bmatrix} \begin{bmatrix} \mathbf{d}_1 \\ \vdots \\ \mathbf{d}_M \end{bmatrix} = \mathbf{b}, \quad (4)$$

where $\mathbf{C}_k = \mathbf{J}_{\omega k}^T \text{Diag}(\mathbf{J}_{\omega k} \ddot{\mathbf{q}}) \in \mathbb{R}^{N \times 3}$ and $\mathbf{b} = \mathbf{f} - \mathbf{g} - \sum_{k=0}^{M-1} m_k \mathbf{J}_k^T \mathbf{J}_k \ddot{\mathbf{q}} \in \mathbb{R}^N$, the sum of all the terms in Equation 2 independent of the inertia matrix. The operator $\text{Diag}(\mathbf{v})$ maps a vector $\mathbf{v} \in \mathbb{R}^n$ to a $\mathbb{R}^{n \times n}$ diagonal matrix whose diagonal is \mathbf{v} . Analyzing the rank of the matrix on the LHS of Equation 4 is too costly. We define a simpler confidence score similar to the one for the mass estimation:

$$w = \sum_{t=0}^{T-1} \sum_{k=0}^{M-1} \sum_{i=0}^2 \left\| \frac{1}{\Delta t} \mathbf{J}_{\omega k}^T \text{Diag}(\mathbf{J}_{\omega k} (\dot{\mathbf{q}}_{t+1} - \dot{\mathbf{q}}_t))(:, i) \right\|$$

c) Confidence score for estimating center of mass

The center of mass (COM) of each body link k affects the equations of motion via the Jacobian \mathbf{J}_k , which maps the generalized velocity $\dot{\mathbf{q}}$ to the Cartesian velocity of COM, \mathbf{v}_k . We can compute \mathbf{v}_k recursively from the Jacobian of its parent joint $\tilde{\mathbf{J}}_k \in \mathbb{R}^{3 \times N}$:

$$\mathbf{v}_k = \tilde{\mathbf{J}}_k \dot{\mathbf{q}} + \mathbf{R}_k [\hat{\mathbf{J}}_{\omega k} \dot{\mathbf{q}}] \mathbf{r}_k = (\tilde{\mathbf{J}}_k - \mathbf{R}_k [\mathbf{r}_k] \hat{\mathbf{J}}_{\omega k}) \dot{\mathbf{q}}, \quad (5)$$

where $\hat{\mathbf{J}}_{\omega k} \in \mathbb{R}^{3 \times N}$ maps the generalized velocity to the angular velocity of link k expressed in the frame of parent joint, \mathbf{R}_k is the transformation from the parent joint frame of link k to the world frame, and \mathbf{r}_k is the COM in the frame of the parent joint of link k . The bracket notation $[\]$ indicates the skew symmetric matrix. By the definition of \mathbf{J}_k and Equation 5,

$$\mathbf{J}_k = \tilde{\mathbf{J}}_k - \mathbf{R}_k [\mathbf{r}_k] \hat{\mathbf{J}}_{\omega k}. \quad (6)$$

The terms in LHS of Equation 2 depending on \mathbf{J}_k can be expressed as

$$m_k \mathbf{J}_k^T (\mathbf{J}_k \ddot{\mathbf{q}} + \dot{\mathbf{J}}_k \dot{\mathbf{q}} - \mathbf{g}_e), \quad (7)$$

substituting \mathbf{J}_k in Equation 7 with Equation 6 and dropping the quadratic terms in \mathbf{r}_k and the constant mass m_k ², we can express the linear terms in \mathbf{r}_k on the LHS of Equation 2 as

$$\begin{aligned} & \left(\tilde{\mathbf{J}}_k^T (\mathbf{R}_k [\hat{\mathbf{J}}_{\omega k} \dot{\mathbf{q}}] + \dot{\mathbf{R}}_k [\hat{\mathbf{J}}_{\omega k} \dot{\mathbf{q}}] + \mathbf{R}_k [\dot{\hat{\mathbf{J}}_{\omega k} \dot{\mathbf{q}}]}) \right. \\ & \left. + \hat{\mathbf{J}}_{\omega k}^T [\mathbf{R}_k^T (\tilde{\mathbf{J}}_k \ddot{\mathbf{q}} + \dot{\tilde{\mathbf{J}}_k} \dot{\mathbf{q}} - \mathbf{g}_e)] \right) \mathbf{r}_k. \end{aligned} \quad (8)$$

To identify COM \mathbf{r}_k for all M links, we need to concatenate the matrix expressed in Equation 8 (inside of the parenthesis) for every link into one single $N \times 3M$ matrix and analyze its rank. Similar to other system parameter estimation, we use a heuristic to approximate the rank.

Let \mathbf{S} be $\mathbf{R}_k [\hat{\mathbf{J}}_{\omega k} \dot{\mathbf{q}}] + \dot{\mathbf{R}}_k [\hat{\mathbf{J}}_{\omega k} \dot{\mathbf{q}}] + \mathbf{R}_k [\dot{\hat{\mathbf{J}}_{\omega k} \dot{\mathbf{q}}}]$ and \mathbf{G} be $[\mathbf{R}_k^T (\tilde{\mathbf{J}}_k \ddot{\mathbf{q}} + \dot{\tilde{\mathbf{J}}_k} \dot{\mathbf{q}} - \mathbf{g}_e)]$, both in $\mathbb{R}^{3 \times 3}$. Expression in 8 can be

²Dropping the quadratic terms can affect the rank analysis and is considered part of approximation by our heuristic.

simplified to $\tilde{\mathbf{J}}_k^T \mathbf{S} + \hat{\mathbf{J}}_{\omega k}^T \mathbf{G}$, which needs to be full column-rank for \mathbf{r}_k to be identifiable. If \mathbf{r}_k is already in the nullspace of \mathbf{S} , multiplying $\tilde{\mathbf{J}}_k^T \in \mathbb{R}^{N \times 3}$ is not going to make \mathbf{r}_k identifiable. The same argument can be made for the \mathbf{G} term. Therefore, we can devise a simple heuristic based on the necessary (not sufficient) condition for every \mathbf{r}_k to be identifiable:

$$w = \sum_{t=0}^T \sum_{k=0}^M \sum_{i=0}^2 \|\mathbf{S}_k(:, i)\| + \|\mathbf{G}_k(:, i)\|$$

d) Confidence score for estimating joint stiffness and damping

The confidence scores for identifying the joint stiffness and damping are much more straightforward. We model the generalized force due to joint stiffness and damping as $\mathbf{f}_{joint}(\mathbf{q}, \dot{\mathbf{q}}; \mu) = -\mathbf{K}_s(\mathbf{q} - \bar{\mathbf{q}}) - \mathbf{K}_d \dot{\mathbf{q}}$, where $\bar{\mathbf{q}}$ is the predefined rest position for the joint angles. The confidence score for the joint stiffness can be computed by:

$$w = \sum_{t=0}^{T-1} \|\mathbf{q}_t - \bar{\mathbf{q}}\|,$$

and the confidence for the joint damping can be computed by:

$$w = \sum_{t=0}^{T-1} \|\dot{\mathbf{q}}_t\|.$$

e) Confidence score for estimating friction

The friction coefficient only affects the motion of the system when there is a sliding contact. We can compute the confidence score by simply measuring the frictional forces occurred in the observed trajectory. Given $(\mathbf{q}_{0:T}, \dot{\mathbf{q}}_{0:T})$, we first perform collision detection and inverse dynamics to approximate the contact points and contact forces. We filter out a subset of contacts \mathcal{C} that have non-zero velocity. The confidence score can be defined as:

$$w = \sum_{\mathbf{p}_i \in \mathcal{C}} \|\mathbf{J}(\mathbf{q}_{t(i)}, \mathbf{p}_i)^T \mathbf{f}_i\|,$$

where $\mathbf{p}_i \in \mathbb{R}^3$ is a contact point in \mathcal{C} , $t(i)$ is the time index when the contact \mathbf{p}_i is active, and \mathbf{f}_i is the corresponding friction force solved by inverse dynamics.

C. Actively controlled system identification

An advantage of our dual-threaded framework is that we can leverage the planning thread to assist the modeling thread when SysID struggles to identify the system parameters for a long time. If the confidence score has been low for N_{his} SysID solutions consecutively, we inform the planning thread to switch its objective function from the main task f_{task} (See IV for detailed definition) to f_{exp} which is designed to explore the range of system behaviors. Conveniently, the confidence score described above can be reused for actively planning a state trajectory that maximizes the parametric excitation for the system parameters of interest. Therefore, we define $f_{exp} = -w(\mathbf{x}_{0:H})$ (Algorithm 1).

Hyper parameters setting					
	Cartpole	InvDP	Arm(COM)	Arm(MOI)	Elastic Rod
ϵ_1	0.1	0.01	0.001	0.001	0.1
ϵ_2	0.5	0.5	0.5	0.5	0.5
T	5	10	5	5	10
H	100	200	100	100	300
Range	[0.2, 5.0]	[0, 0.5]	[0, 0.05]	[0, 0.2]	[0, 15]

TABLE I: Hyper parameters for our experiments. InvDP is an abbreviation for inverted double pendulum. ϵ_1 is the threshold for detecting parameter changes, ϵ_2 is the threshold of confidence, T is the trajectory length used to solve each system identification problem, and H is the horizon for each iLQR optimization. The unknown parameters are randomly sampled in the ranges shown here. The range of COM and MOI are determined by geometric boundary of the robot arm.

IV. Evaluation

We implemented our method using off-the-shelf differentiable physics engine, NimblePhysics [41] based on DART [22]. We evaluate the method on four dynamic motor control tasks in which the robot needs to continuously identify the system parameters and solve for the control trajectories. We compare our methods to four different baselines:

- 1) **Naive**: Solve SysID using the most recent observations. Solve control using MPC-iLQR.
- 2) **Smooth**: Solve SysID using the average of five previously solved system parameters. Solve control using MPC-iLQR.
- 3) **Weighted**: Solve SysID using Equation 1 with five previously solved system parameters. Solve control using MPC-iLQR. This baseline is the same as our method except that the most recent solution is always accepted and interpolated with the current solution.
- 4) **UP-OSI**: Use an MLP model trained offline for SysID. Control the robot using a system-parameter-conditioned policy trained offline using deep RL approach. We use the implementation by [44].

On the control side, we also evaluate the effectiveness of adaptive horizon starting time for the planning thread. The optimal control problem for all four tasks share the same form for their objective functions:

$$f_{task}(\mathbf{x}_{0:H}, \mathbf{u}_{0:H-1}) = \frac{1}{2} \sum_k^{H-1} (\mathbf{x}_k - \bar{\mathbf{x}})^T \mathbf{Q}_r (\mathbf{x}_k - \bar{\mathbf{x}}) + \frac{1}{2} (\mathbf{x}_H - \bar{\mathbf{x}})^T \mathbf{Q}_f (\mathbf{x}_H - \bar{\mathbf{x}}) + \frac{1}{2} \sum_k^{H-1} \mathbf{u}_k^T \mathbf{R} \mathbf{u}_k, \quad (9)$$

where $\bar{\mathbf{x}}$ is the target state, \mathbf{R} is the cost weights for an action, \mathbf{Q}_r defines the running cost weights for a state, and \mathbf{Q}_f defines the cost weights for the final state. In the four tasks we demonstrated, we found that only one example, the elastic rod moving task, triggers the active system identification mode in which the objective function for iLQR switched to $f_{exp} = -w(\mathbf{x}_{0:H})$.

To bring the simulated environment closer to the real-world, we simulate sensing and actuating errors by adding random

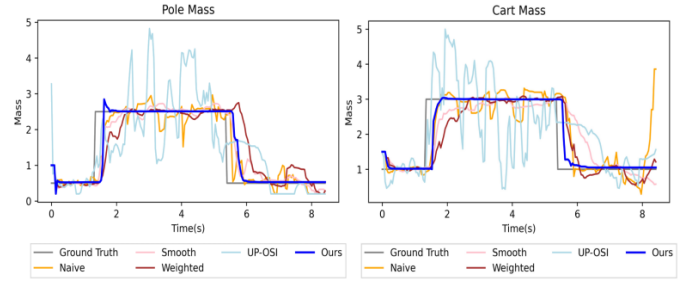


Fig. 3: Identifying masses for the cartpole experiment.

Time (second) required to reach control objective				
	Cartpole	InvDP	Robot Arm	Elastic Rod
Ours	6.31(0.42)	3.53(0.22)	2.10(0.20)	4.60(0.07)
Weighted	6.76(0.45)	3.73(0.46)	2.53(0.05)	6.42(1.06)
Smooth	6.98(0.62)	3.80(0.44)	2.76(0.07)	6.70(2.57)
Naive	7.57(0.87)	4.26(0.61)	3.01(0.10)	9.05(4.08)
UP-OSI	Failed	6.23(0.75)	NA	NA

TABLE II: Time required to complete the control task. Mean and standard deviation over 5 experiments with different random seeds are reported. A trial is considered successful if it reaches a state less than 0.1 l2-distance from the target state within 1000 time steps. We only compared with UP-OSI on the tasks implemented in their public codebase.

noise in the observed states, as well as in the actions being executed. All the hyper parameters are reported in Table I.

A. Swing-Up cartpole with unknown masses

We started with a classical motor control problem: swing up and balance a pole attached to a cart by applying a linear force to the cart to reach a desired position at the end. The objective function is defined by Equation 9 with $\mathbf{R} = 0.01$, $\mathbf{Q}_r = \mathbf{0}$, and $\mathbf{Q}_f = \text{Diag}([10, 50, 10, 10])$. The target $\bar{\mathbf{x}} = [1, 0, 0, 0]$ requires the pole to be balanced at the configuration (1, 0) with zero velocity as quickly as possible.

The mass of the cart and the mass of the pole are unknown initially and can change occasionally. Figure 3 shows the accuracy and stability of our method compared against the baselines. Our method can quickly identify the correct masses and respond rapidly to the parameter change. We further demonstrated that more effective SysID positively impacts the quality of control. Table II shows that the time required for our MPC-iLQR controller to complete the task. Our controller is significantly more effective than baselines based on the same MPC-iLQR. UP-OSI was not able to complete the task after 1000 time steps, suggesting that the MLP-based SysID can be brittle when the changes in parameters result in out-of-distribution state trajectories (See the accompanying video for interactive demos).

B. Inverted double pendulum with unknown damping coefficients

This task is the same as the cart-pole, but an additional unactuated pole segment makes the double inverted pendulum a more challenging control problem. The cost function is defined

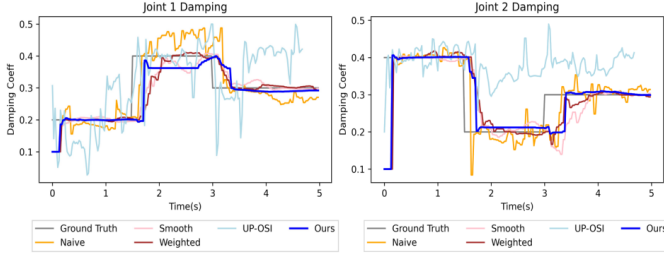


Fig. 4: Identifying damping coefficients for the double inverted pendulum experiment.

by Equation 9 with $\mathbf{Q}_f = \text{Diag}([10, 50, 10, 10, 10, 10])$, $\mathbf{Q}_r = \mathbf{0}$, and $\mathbf{R} = 0.01$. The target state $\bar{\mathbf{x}}$ is set to be $[0, 0, 0, 0, 0, 0]$ which requires the double inverted pendulum to be balanced at zero configuration with zero velocity as quickly as possible.

The damping coefficients of the two revolute joints are unknown. Figure 4 shows that these parameters can be more accurately identified by our method compared to the baselines. We further demonstrated that the accuracy of SysID plays a significant role in control. Table II shows the time required to complete the task. Our method again outperforms other baselines.

C. Rokae Xmate3 with unknown end-effector mass distribution

Robot manipulators often encounter objects with unknown mass and unknown mass distribution. While the mass of the object is simple to obtain from force sensors, estimating the center of mass and the moment of inertia of the object is more challenging. Furthermore, for objects like a bag of sand or a jar of water, the center of mass and the moment of inertia could change over time and need to be estimated in an online fashion.

In this example, a Rokae xmate3 robotic arm is required to carry an object from the initial configuration of the robot to a final configuration (Figure 6). The COM and the moment of inertia of the object is unknown and could change over time. The cost function is defined by Equation 9 with $\mathbf{R} = \text{Diag}([0.2, 0.2, 0.2])$, $\mathbf{Q}_r = \text{Diag}([0.1, 0.1, 0.1, 0.0, 0])$, and $\mathbf{Q}_f = \text{Diag}([100, 100, 500, 50, 50, 50])$.

We assumed that the object is welded to the end-effector of the robot and directly changed the COM and the moment of inertia of the end-effector during the experiment. Figure 5 shows that our adaptive SysID outperforms all the baselines. Similarly, the accurate estimation of the system parameters has a positive impact on control, as shown in Table II.

D. Moving elastic rod with unknown elasticity

This example involves an elastic rod modeled by four rigid links connected by revolute joints with internal springs (Figure 8). The task is to push the base link of the elastic rod to the target location as quickly as possible, while keeping the rod straight and vertical when hitting the target. Intuitively if the rod is stiff, we can apply relatively large acceleration to the base. If the rod is more elastic, then we have to accelerate strategically

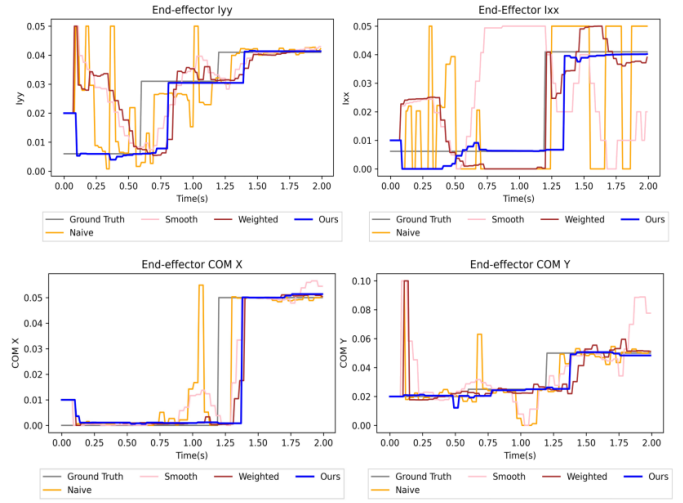


Fig. 5: Identifying the center of mass and the moment of inertia for Rokae Xmates3 robot arm. Since the end-effector cannot rotate in the roll direction, we only show the identification result around X and Y axis.

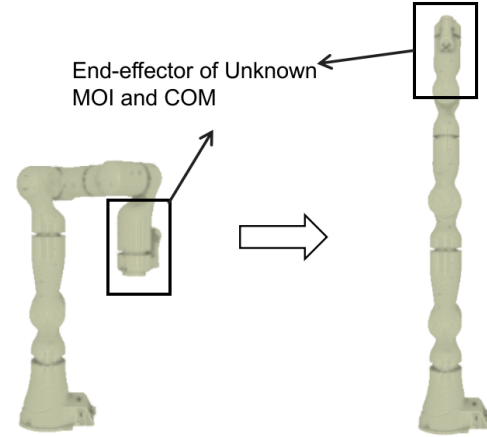


Fig. 6: Rokae xmate3 robot arm: The robot needs to move from the initial configuration to the final one with initially unknown and changing COM and the moment of inertia in its end-effector.

to mitigate bending. Accurate estimation of spring stiffness is crucial to control the rod optimally. The cost function is defined by Equation 9 with $\mathbf{Q}_r = \text{Diag}([0.1, 0.1, 0.1, 0.1, 0, 0, 0, 0])$ and $\mathbf{Q}_f = \text{Diag}([100, 100, 100, 100, 50, 100, 100, 100])$ and $\mathbf{R} = 0.001$. The target is set at $\bar{\mathbf{x}} = [2.5, 0, 0, 0, 0, 0, 0, 0]$.

This is an example that benefits from the coordination of the modeling thread and the planning thread, such that correct parameters can be identified and the task can be accomplished optimally. At the beginning, the iLQR with underestimated joint stiffness parameters produces slow actions in the hope of keep the rod straightened at the target. However, these conservative actions failed to excite the system and prevented the joint stiffness from being identified. Our confidence score correctly

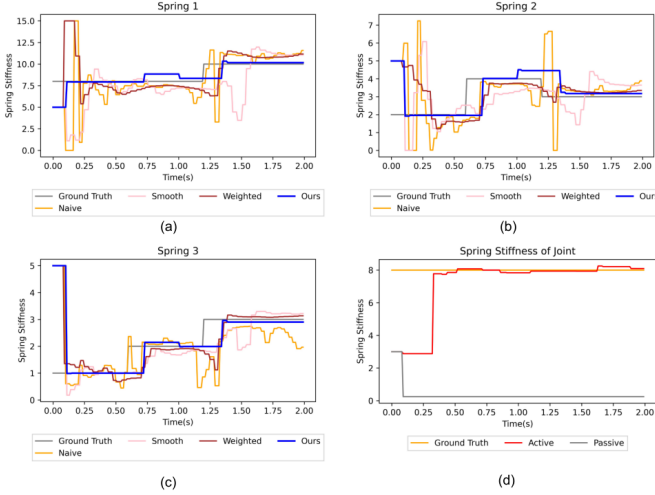


Fig. 7: (a)-(c): Identifying the spring stiffness for the elastic rod. (d): System identification with and without active SysID control.

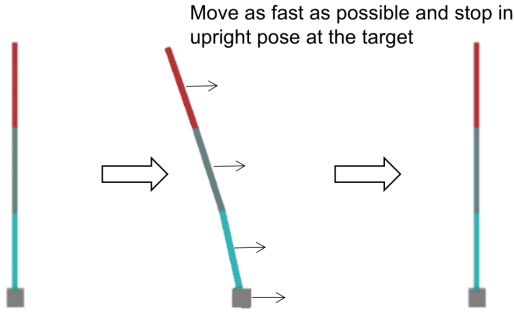


Fig. 8: Moving elastic rod with unknown elasticity.

exposed the issue and switched to the actively controlled SysID mode. Fig 7 (d) shows that active SysID quickly corrects the joint stiffness and switches back to optimizing the task objective, resulting in a more optimal control sequence at the end. Using active SysID control, the average time to reach the target can be further decreased from 6.10 seconds to 4.028 seconds.

We compare these results with the baselines and 7 show that our method can identify the elasticity of the rod accurately and respond quickly to the change of the parameters. Noticeably the **Weighted** baseline also performs better than other baselines, suggesting that our confidence score is effective even with a simple moving average scheme. The result for control is shown in Table II.

E. Ablation study on adaptive starting time

We also evaluated the impact of adaptive starting time of the horizon for the planning thread on the cart-pole example. We replace our adaptive method with a fixed starting time. To pick a reasonable fixed starting time, we use the average time required to solve an iLQR optimization over the entire trajectory. Over five experiment trials, we found that the fixed starting time on average takes 8.20 seconds to swing up and balance the

cartpole with two failed cases, whereas our method on average takes 6.31 seconds to swing up and balance with no failure cases. See the supplementary video for all the experiments.

V. Conclusion

We present a method for continuous improvement of modeling and control after deploying the robot to the target environment. We develop a differentiable physics simulation framework that performs online motion planning and system identification simultaneously in real-time. Our online system identification algorithm is robust against noisy and faulty observations and is able to detect changes in the environments in real-time. Our model predictive control adaptively adjusts the optimizing window to ensure effective real-time control.

Reliably optimizing complex trajectories in the presence of contacts remains an exciting area for future exploration. While in principle our method can be trivially applied to scenarios involving planning through contact, in practice the convergence of the iLQR planner becomes highly variable, both in time required and in quality of solution. More robust planning algorithms that can handle dynamic contact can be substituted into our method as they are developed, to allow for robust parameter-varying control through contact. Beside friction coefficient, more parameters related to contact such as restitution coefficient may worth exploring similar heuristics to accelerate system identification.

Testing our proposed method on a physical robot also remains as future work. While we have successfully run our planning and system identification threads in parallel and in real time against a simulated world, which means no fundamental timing or methodological barriers remain, mechanical experiment design and manufacture are left to future work.

Acknowledgments

References

- [1] Karl Johan Åström and Peter Eykhoff. System identification—a survey. *Automatica*, 7(2):123–162, 1971.
- [2] Paul F. Christiano, Zain Shah, Igor Mordatch, Jonas Schneider, Trevor Blackwell, Joshua Tobin, Pieter Abbeel, and Wojciech Zaremba. Transfer from simulation to real world through learning deep inverse dynamics model. *CoRR*, abs/1610.03518, 2016. URL <http://arxiv.org/abs/1610.03518>.
- [3] Filipe de Avila Belbute-Peres, Kevin A. Smith, Kelsey R. Allen, Josh Tenenbaum, and J. Zico Kolter. End-to-end differentiable physics for learning and control. In Samy Bengio, Hanna M. Wallach, Hugo Larochelle, Kristen Grauman, Nicolò Cesa-Bianchi, and Roman Garnett, editors, *Advances in Neural Information Processing Systems 31: Annual Conference on Neural Information Processing Systems 2018, NeurIPS 2018*, pages 7178–7189, 2018. URL <https://proceedings.neurips.cc/paper/2018/hash/842424a1d0595b76ec4fa03c46e8d755-Abstract.html>.
- [4] Jonas Degraeve, Michiel Hermans, Joni Dambre, and Francis Wyffels. A differentiable physics engine for

- deep learning in robotics. *Frontiers Neurorobotics*, 13: 6, 2019. doi: 10.3389/fnbot.2019.00006. URL <https://doi.org/10.3389/fnbot.2019.00006>.
- [5] Feng Ding, Xuehai Wang, Qijia Chen, and Yongsong Xiao. Recursive least squares parameter estimation for a class of output nonlinear systems based on the model decomposition. *Circuits, Systems, and Signal Processing*, 35(9):3323–3338, 2016.
- [6] Ioannis Exarchos, Yifeng Jiang, Wenhao Yu, and C. Karen Liu. Policy transfer via kinematic domain randomization and adaptation. *CoRR*, abs/2011.01891, 2020. URL <https://arxiv.org/abs/2011.01891>.
- [7] Moritz Geilinger, David Hahn, Jonas Zehnder, Moritz Bächer, Bernhard Thomaszewski, and Stelian Coros. ADD: analytically differentiable dynamics for multi-body systems with frictional contact. *ACM Trans. Graph.*, 39(6):190:1–190:15, 2020. doi: 10.1145/3414685.3417766. URL <https://doi.org/10.1145/3414685.3417766>.
- [8] David Hahn, Pol Banzet, James M. Bern, and Stelian Coros. Real2sim: visco-elastic parameter estimation from dynamic motion. *ACM Trans. Graph.*, 38(6):236:1–236:13, 2019. doi: 10.1145/3355089.3356548. URL <https://doi.org/10.1145/3355089.3356548>.
- [9] Nicolas Heess, Jonathan J. Hunt, Timothy P. Lillicrap, and David Silver. Memory-based control with recurrent neural networks. *CoRR*, abs/1512.04455, 2015. URL <http://arxiv.org/abs/1512.04455>.
- [10] Eric Heiden, Miles Macklin, Yashraj S. Narang, Dieter Fox, Animesh Garg, and Fabio Ramos. Disect: A differentiable simulation engine for autonomous robotic cutting. In *Robotics: Science and Systems XVII, Virtual Event, July 12-16, 2021*, 2021. doi: 10.15607/RSS.2021.XVII.067. URL <https://doi.org/10.15607/RSS.2021.XVII.067>.
- [11] Eric Heiden, David Millard, Erwin Coumans, Yizhou Sheng, and Gaurav S. Sukhatme. Neursim: Augmenting differentiable simulators with neural networks. In *IEEE International Conference on Robotics and Automation, ICRA 2021, Xi'an, China, May 30 - June 5, 2021*, pages 9474–9481. IEEE, 2021. doi: 10.1109/ICRA48506.2021.9560935. URL <https://doi.org/10.1109/ICRA48506.2021.9560935>.
- [12] Philipp Holl, Nils Thuerey, and Vladlen Koltun. Learning to control pdes with differentiable physics. In *8th International Conference on Learning Representations, ICLR 2020*. OpenReview.net, 2020. URL <https://openreview.net/forum?id=HyeSin4FPB>.
- [13] Yuanming Hu, Jiancheng Liu, Andrew Spielberg, Joshua B. Tenenbaum, William T. Freeman, Jiajun Wu, Daniela Rus, and Wojciech Matusik. Chainqueen: A real-time differentiable physical simulator for soft robotics. *CoRR*, abs/1810.01054, 2018. URL <http://arxiv.org/abs/1810.01054>.
- [14] Yuanming Hu, Luke Anderson, Tzu-Mao Li, Qi Sun, Nathan Carr, Jonathan Ragan-Kelley, and Frédo Durand. DiffTaichi: Differentiable programming for physical simulation. In *8th International Conference on Learning Representations, ICLR 2020, Addis Ababa, Ethiopia, April 26-30, 2020*. OpenReview.net, 2020. URL <https://openreview.net/forum?id=B1eB5xSFvr>.
- [15] Zhiao Huang, Yuanming Hu, Tao Du, Siyuan Zhou, Hao Su, Joshua B. Tenenbaum, and Chuang Gan. Plasticinelab: A soft-body manipulation benchmark with differentiable physics. In *9th International Conference on Learning Representations, ICLR 2021*. OpenReview.net, 2021. URL <https://openreview.net/forum?id=xCcdBRQEDW>.
- [16] Jemin Hwangbo, Joonho Lee, Alexey Dosovitskiy, Dario Bellicoso, Vassilios Tsounis, Vladlen Koltun, and Marco Hutter. Learning agile and dynamic motor skills for legged robots. *CoRR*, abs/1901.08652, 2019. URL <http://arxiv.org/abs/1901.08652>.
- [17] Yifeng Jiang, Tingnan Zhang, Daniel Ho, Yunfei Bai, C. Karen Liu, Sergey Levine, and Jie Tan. Simgan: Hybrid simulator identification for domain adaptation via adversarial reinforcement learning. In *IEEE International Conference on Robotics and Automation, ICRA 2021, Xi'an, China, May 30 - June 5, 2021*, pages 2884–2890. IEEE, 2021. doi: 10.1109/ICRA48506.2021.9561731. URL <https://doi.org/10.1109/ICRA48506.2021.9561731>.
- [18] Michael Kaess, Ananth Ranganathan, and Frank Dellaert. isam: Incremental smoothing and mapping. *IEEE Trans. Robotics*, 24(6):1365–1378, 2008. doi: 10.1109/TRO.2008.2006706. URL <https://doi.org/10.1109/TRO.2008.2006706>.
- [19] Junggon Kim. Lie group formulation of articulated rigid body dynamics. 2012.
- [20] Gerhard Kreisselmeier and Brian Anderson. Robust model reference adaptive control. *IEEE Transactions on Automatic Control*, 31(2):127–133, 1986.
- [21] Quentin Le Lidec, Igor Kalevatykh, Ivan Laptev, Cordelia Schmid, and Justin Carpentier. Differentiable simulation for physical system identification. *IEEE Robotics and Automation Letters*, 6(2):3413–3420, 2021. doi: 10.1109/LRA.2021.3062323.
- [22] Jeongseok Lee, Michael X. Grey, Sehoon Ha, Tobias Kunz, Sumit Jain, Yuting Ye, Siddhartha S. Srinivasa, Mike Stilman, and C. Karen Liu. DART: dynamic animation and robotics toolkit. *J. Open Source Softw.*, 3(22):500, 2018. doi: 10.21105/joss.00500. URL <https://doi.org/10.21105/joss.00500>.
- [23] Weiwei Li and Emanuel Todorov. Iterative linear quadratic regulator design for nonlinear biological movement systems. In Helder Araújo, Alves Vieira, José Braz, Bruno Encarnação, and Marina Carvalho, editors, *ICINCO 2004, Proceedings of the First International Conference on Informatics in Control, Automation and Robotics*, pages 222–229. INSTICC Press, 2004.
- [24] Junbang Liang, Ming C. Lin, and Vladlen Koltun. Differentiable cloth simulation for inverse problems. In Hanna M. Wallach, Hugo Larochelle, Alina Beygelzimer, Florence d’Alché-Buc, Emily B. Fox, and Roman Garnett, editors, *Advances in Neural Information Processing Systems 32: Annual Conference on Neural Information*

- Processing Systems 2019*, pages 771–780, 2019. URL <https://proceedings.neurips.cc/paper/2019/hash/28f0b864598a1291557bed248a998d4e-Abstract.html>.
- [25] Michael Lutter, Johannes Silberbauer, Joe Watson, and Jan Peters. A differentiable newton euler algorithm for multi-body model learning. *ArXiv*, abs/2010.09802, 2020.
- [26] By DAVID MAYNE. A second-order gradient method for determining optimal trajectories of non-linear discrete-time systems. *International Journal of Control*, 3(1): 85–95, 1966. doi: 10.1080/00207176608921369. URL <https://doi.org/10.1080/00207176608921369>.
- [27] Michael Neunert, Thiago Boaventura, and Jonas Buchli. Why off-the-shelf physics simulators fail in evaluating feedback controller performance—a case study for quadrupedal robots. In *Advances in Cooperative Robotics*, pages 464–472. World Scientific, 2017.
- [28] OpenAI, Ilge Akkaya, Marcin Andrychowicz, Maciek Chociej, Mateusz Litwin, Bob McGrew, Arthur Petron, Alex Paino, Matthias Plappert, Glenn Powell, Raphael Ribas, Jonas Schneider, Nikolas Tezak, Jerry Tworek, Peter Welinder, Lilian Weng, Qiming Yuan, Wojciech Zaremba, and Lei Zhang. Solving rubik’s cube with a robot hand. *CoRR*, abs/1910.07113, 2019. URL <http://arxiv.org/abs/1910.07113>.
- [29] Patric Parks. Lyapunov redesign of model reference adaptive control systems. *IEEE Transactions on Automatic Control*, 11(3):362–367, 1966.
- [30] Xue Bin Peng, Marcin Andrychowicz, Wojciech Zaremba, and Pieter Abbeel. Sim-to-real transfer of robotic control with dynamics randomization. *CoRR*, abs/1710.06537, 2017. URL <http://arxiv.org/abs/1710.06537>.
- [31] Xue Bin Peng, Erwin Coumans, Tingnan Zhang, Tsang-Wei Edward Lee, Jie Tan, and Sergey Levine. Learning agile robotic locomotion skills by imitating animals. In Marc Toussaint, Antonio Bicchi, and Tucker Hermans, editors, *Robotics: Science and Systems XVI, Virtual Event / Corvallis, Oregon, USA, July 12-16, 2020*, 2020. doi: 10.15607/RSS.2020.XVI.064. URL <https://doi.org/10.15607/RSS.2020.XVI.064>.
- [32] Samuel Pfrommer, Mathew Halm, and Michael Posa. Contactnets: Learning discontinuous contact dynamics with smooth, implicit representations. In *4th Conference on Robot Learning, CoRL 2020, 16-18 November 2020*, volume 155 of *Proceedings of Machine Learning Research*, pages 2279–2291. PMLR, 2020. URL <https://proceedings.mlr.press/v155/pfrommer21a.html>.
- [33] Yi-Ling Qiao, Junbang Liang, Vladlen Koltun, and Ming C. Lin. Scalable differentiable physics for learning and control. In *Proceedings of the 37th International Conference on Machine Learning, ICML 2020, 13-18 July 2020, Virtual Event*, volume 119 of *Proceedings of Machine Learning Research*, pages 7847–7856. PMLR, 2020. URL <http://proceedings.mlr.press/v119/qiao20a.html>.
- [34] Yi-Ling Qiao, Junbang Liang, Vladlen Koltun, and Ming C. Lin. Efficient differentiable simulation of articulated bodies. In *Proceedings of the 38th International Conference on Machine Learning, ICML 2021*, volume 139 of *Proceedings of Machine Learning Research*, pages 8661–8671. PMLR, 2021. URL <http://proceedings.mlr.press/v139/qiao21a.html>.
- [35] Connor Schenck and Dieter Fox. Spnets: Differentiable fluid dynamics for deep neural networks. In *2nd Annual Conference on Robot Learning, CoRL 2018, Zürich, Switzerland, 29-31 October 2018, Proceedings*, volume 87 of *Proceedings of Machine Learning Research*, pages 317–335. PMLR, 2018. URL <http://proceedings.mlr.press/v87/schenck18a.html>.
- [36] István Szita, Bálint Takács, and András Lörincz. ε -mdps: Learning in varying environments. *J. Mach. Learn. Res.*, 3(null):145–174, March 2003. ISSN 1532-4435. doi: 10.1162/153244303768966148. URL <https://doi.org/10.1162/153244303768966148>.
- [37] Jie Tan, Tingnan Zhang, Erwin Coumans, Atil Iscen, Yunfei Bai, Danijar Hafner, Steven Bohez, and Vincent Vanhoucke. Sim-to-real: Learning agile locomotion for quadruped robots. *CoRR*, abs/1804.10332, 2018. URL <http://arxiv.org/abs/1804.10332>.
- [38] Linh Vu and Daniel Liberzon. Common lyapunov functions for families of commuting nonlinear systems. *Syst. Control. Lett.*, 54(5):405–416, 2005. doi: 10.1016/j.sysconle.2004.09.006. URL <https://doi.org/10.1016/j.sysconle.2004.09.006>.
- [39] Andreas Wächter and Lorenz T. Biegler. On the implementation of an interior-point filter line-search algorithm for large-scale nonlinear programming. *Mathematical Programming*, 106:25–57, 2006.
- [40] Kun Wang, Mridul Aanjaneya, and Kostas E. Bekris. Sim2sim evaluation of a novel data-efficient differentiable physics engine for tensegrity robots. In *IEEE/RSJ International Conference on Intelligent Robots and Systems, IROS 2021, Prague, Czech Republic, September 27 - Oct. 1, 2021*, pages 1694–1701. IEEE, 2021. doi: 10.1109/IROS51168.2021.9636783. URL <https://doi.org/10.1109/IROS51168.2021.9636783>.
- [41] Keenon Werling, Dalton Omens, Jeongseok Lee, Ioannis Exarchos, and C. Karen Liu. Fast and feature-complete differentiable physics for articulated rigid bodies with contact. *CoRR*, abs/2103.16021, 2021. URL <https://arxiv.org/abs/2103.16021>.
- [42] Jie Xu, Tao Chen, Lara Zlokapa, Michael Foshey, Wojciech Matusik, Shinjiro Sueda, and Pulkit Agrawal. An end-to-end differentiable framework for contact-aware robot design. In *Robotics: Science and Systems XVII, 2021*, 2021. doi: 10.15607/RSS.2021.XVII.008. URL <https://doi.org/10.15607/RSS.2021.XVII.008>.
- [43] Zhuo Xu, Wenhao Yu, Alexander Herzog, Wenlong Lu, Chuyuan Fu, Masayoshi Tomizuka, Yunfei Bai, C. Karen Liu, and Daniel Ho. COCOI: contact-aware online context inference for generalizable non-planar pushing. *CoRR*, abs/2011.11270, 2020. URL <https://arxiv.org/abs/2011.11270>.
- [44] Wenhao Yu, C. Karen Liu, and Greg Turk. Preparing

for the unknown: Learning a universal policy with online system identification. *CoRR*, abs/1702.02453, 2017. URL <http://arxiv.org/abs/1702.02453>.

- [45] Miguel Zamora, Momchil Peychev, Sehoon Ha, Martin T. Vechev, and Stelian Coros. PODS: policy optimization via differentiable simulation. In *Proceedings of the 38th International Conference on Machine Learning, ICML 2021*, volume 139 of *Proceedings of Machine Learning Research*, pages 7805–7817. PMLR, 2021. URL <http://proceedings.mlr.press/v139/mora21a.html>.
- [46] Yaofeng Desmond Zhong, Biswadip Dey, and Amit Chakraborty. Extending lagrangian and hamiltonian neural networks with differentiable contact models. In A. Beygelzimer, Y. Dauphin, P. Liang, and J. Wortman Vaughan, editors, *Advances in Neural Information Processing Systems*, 2021. URL <https://openreview.net/forum?id=pZQrKCKbas>.

VI. Appendix

A. Details of MPC-iLQR Algorithm

We show the algorithm of our implementation of MPC-iLQR in Algorithm 2. Please see [23] for detailed derivation of iLQR. \mathbf{u}_t is control force at time t , and $\mathbf{K}_t, \mathbf{k}_t$ are feedback and feedforward gain in iLQR algorithm. We use warm start for iLQR trajectory optimizer. At the beginning of the algorithm, the buffer for state, action, feedback and feedforward gain are initialized using last iLQR buffer with obsolete terms discarded. When deploying the algorithm, we use $\tilde{\mathbf{u}}_t = \mathbf{u}_t + \mathbf{K}_t \mathbf{x}_t + \mathbf{k}_t$ to compute control forces $\tilde{\mathbf{u}}_t$ based on actual observed state \mathbf{x}_t .

B. Coriolis terms

Coriolis and centrifugal forces can be added to the computation of the confidence score in mass and moment of inertia

estimation. Our method achieves good results without including this term, but it might improve the results for more dynamic and complex examples.

$$\mathbf{c}(\mathbf{q}, \dot{\mathbf{q}}; \boldsymbol{\mu}) = m_k (\mathbf{J}_k^T \dot{\mathbf{J}}_k + \mathbf{J}_{\omega_k}^T \tilde{\mathbf{I}} \mathbf{J}_k + \mathbf{J}_{\omega_k}^T [\boldsymbol{\omega}] \tilde{\mathbf{I}} \mathbf{J}_{\omega_k}) \dot{\mathbf{q}}$$

For mass, we can add $(\mathbf{J}_k^T \dot{\mathbf{J}}_k + \mathbf{J}_{\omega_k}^T \tilde{\mathbf{I}} \mathbf{J}_k + \mathbf{J}_{\omega_k}^T [\boldsymbol{\omega}] \tilde{\mathbf{I}} \mathbf{J}_{\omega_k}) \dot{\mathbf{q}}$ as additional term after each $\mathbf{B}(:, k)$. For moment of inertia, we can add $\mathbf{J}_{\omega_k}^T [\boldsymbol{\omega}] \text{Diag}(\mathbf{J}_{\omega_k} \dot{\mathbf{q}})$ after each \mathbf{C}_k , $\boldsymbol{\omega}_k = \mathbf{J}_{\omega_k} \dot{\mathbf{q}}$.

Algorithm 2: MPC-iLQR

Input: $\mathbf{x}_{\hat{t}}, \bar{\boldsymbol{\mu}}, f, H, \epsilon, N_{\text{maxiter}}$

$i = 0$

$C_{\text{old}}, C_{\text{new}} = \text{Inf}$

▷ Initialize from last optimization

$H_{\text{last remain}} \leftarrow t_{\text{last end}} - \hat{t}$

$\mathbf{u}_{\hat{t}:\hat{t}+H_{\text{last remain}}} \leftarrow \mathbf{u}_{t_{\text{last end}}-t_{\text{last remain}}}$

$\mathbf{k}_{\hat{t}:\hat{t}+H_{\text{last remain}}} \leftarrow \mathbf{k}_{t_{\text{last end}}-t_{\text{last remain}}}$

$\mathbf{K}_{\hat{t}:\hat{t}+H_{\text{last remain}}} \leftarrow \mathbf{K}_{t_{\text{last end}}-t_{\text{last remain}}}$

$\mathbf{x}_{\hat{t}:\hat{t}+H_{\text{last remain}}} \leftarrow \mathbf{x}_{t_{\text{last end}}-t_{\text{last remain}}}$

▷ Optimize trajectory using iLQR:

while $i < N_{\text{maxiter}}$ **do**

$C_{\text{new}}, \mathbf{x}_{\hat{t}:\hat{t}+H}, \mathbf{A}_{\hat{t}:\hat{t}+H}, \mathbf{B}_{\hat{t}:\hat{t}+H} \leftarrow$

 iLQRForward($\bar{\boldsymbol{\mu}}, f$)

$\mathbf{u}_{\hat{t}:\hat{t}+H-1}, \mathbf{k}_{\hat{t}:\hat{t}+H-1}, \mathbf{K}_{\hat{t}:\hat{t}+H-1} \leftarrow$

 iLQRBackward(f)

if $|C_{\text{new}} - C_{\text{old}}| \leq \epsilon$ **then**

Terminate

$C_{\text{old}} \leftarrow C_{\text{new}}$

$i \leftarrow i + 1$
